GSA Data Repository Figure Captions

Figure S1. Schematic representation $^{87}Sr/^{86}Sr$ sources of uncertainty on individual data points. Six sources of uncertainty are identified in our Ordovician samples. The range of values is approximate and in many cases poorly constrained in terms of variation estimates (e.g., diagenesis, sample impurities, global seawater homogeneity in the Ordovician).

Figure S2.a-c. Conodonts from the Antelope Range section in Nevada (see Table S1). Width between lines (forming a box) shown in slide is 3.5 mm. **a.** sample 5-25-82AI, mixture of rastrate forms transitional between coniform and ramiform conodont elements, and blade-type conodonts. **b.** sample 5-25-82J, mixture of single cone (coniform)- type conodonts. **c.** sample 5-25-82R, mixture of coniform and ramiform (denticulate) conodonts.

Figure S3. $^{87}Sr/^{86}Sr$ for the Hainesville, WV and Row Park, MD sections (see Boger, 1976). Values corroborate that seen in the same time interval in other sections. These data are not plotted in Fig. 11 in the paper, but are listed in Table S2 – supplementary data.

Figure S4. $^{87}Sr/^{86}Sr$ for the Marble Hollow section in Tennessee together with conodont species range data (Bergström, 1973). Data are plotted in Fig. 11 in the paper.

Figure S5. $^{87}Sr/^{86}Sr$ for the Yellow Creek core in Mississippi (see Dwyer, 1996; Dwyer and Repetski, 2012). Data are plotted in Fig. 11 in the paper.

Figure S6. $^{87}Sr/^{86}Sr$ for the East River Mountain section in West Virginia together with conodont species range data and K-bentonite radiometric age (Leslie et al., 2012). Data point is plotted in Fig. 11 in the paper.

Figure S7. $^{87}Sr/^{86}Sr$ for the New Point core in Indiana (see Dwyer, 1996). Data are plotted in Fig. 11 in the paper.

Figure S8. $^{87}Sr/^{86}Sr$ vs. Sr concentration (ppm) for conodont samples analyzed here (note that not all conodonts in Dwyer, 1996 include concentration data) emphasizing that Sr concentrations are much greater than expected from a consideration of the Sr partition coefficient in biogenic apatite (and much higher than the Sr concentrations in living marine fish teeth today) (see Holmden et al., 1996). As discussed by Holmden et al. (1996) this is likely because most of the Sr in the conodont apatite is incorporated post-mortem, at the sediment water interface, and during early diagenesis. Although it may eventually be possible to use the high concentrations as a screening tool for best preserved samples for reconstructing seawater $^{87}Sr/^{86}Sr$, it appears that older samples in our study have higher concentrations of Sr. The reasons for this are not yet known by us.

Figure S9. Plots showing direct comparisons between our $^{87}Sr/^{86}Sr$ data and McArthur et al. (2012). **a.** This is simply a larger version of the inset plotted in our paper Fig. 11 with $^{87}Sr/^{86}Sr$ trend for all sections studied and calibrated to the Geologic Time Scale 2012 (Cooper and Sadler, 2012). LOWESS fit curve (in red) for the Ordovician from McArthur et al. (2012) plotted over our data are calibrated to the same age model of Cooper and Sadler (2012). Our data are corrected to a preferred value for SRM 987 standard of 0.710245 (see text for discussion and GSA Data Repository Tables S1, S3), which is essentially the same as McArthur et al. (2012) who use 0.710248. The fact that much of our data is less radiogenic for a given time period compared to McArthur et al. (2012) could be a result of systematic differences in how individual samples were assigned ages using biostratigraphy or could reflect real differences in how conodonts and brachiopods preserve seawater $^{87}Sr/^{86}Sr$. **b.** This represents a scanned image of the Ordovician portion of the McArthur et al. (2012) $^{87}Sr/^{86}Sr$ curve with density of sampling shown relative to data plotted in our paper Fig. 11 (green dots) (note that our smaller data sets - Meiklejohn Peak, Marble Hollow, Yellow Creek, and East River Mountain – were not plotted here).

SUPPLEMENTARY DATA REPOSITORY

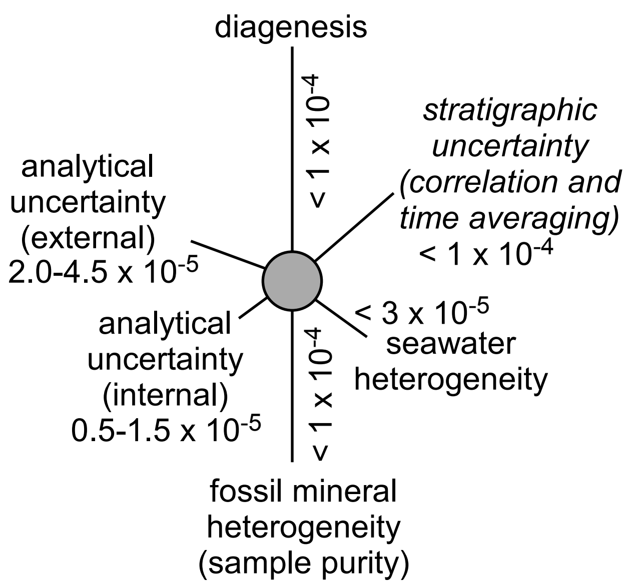

Fig. S1, Saltzman et al

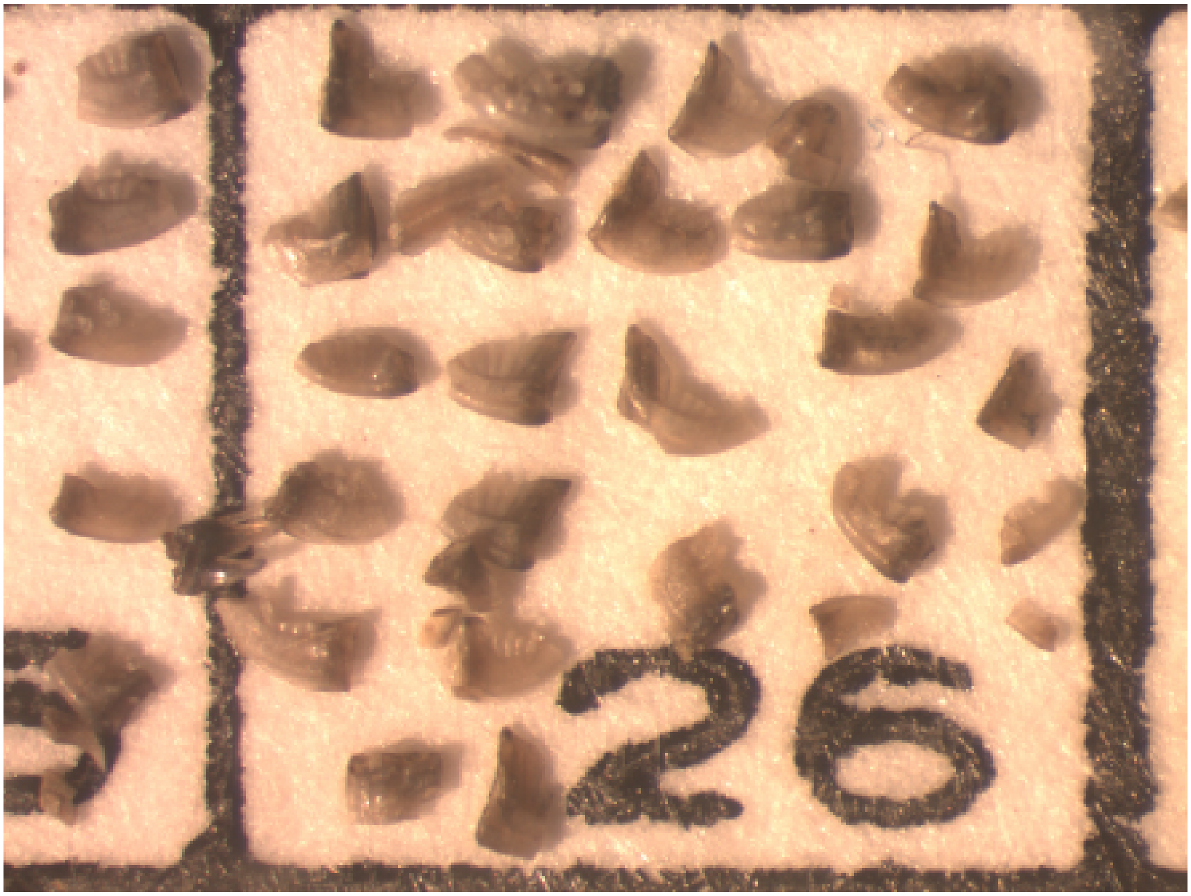

Fig. S2.a Antelope Range sample 5-25-82AI

Fig. S2.b. Antelope Range sample 5-25-82J
Saltzman et al

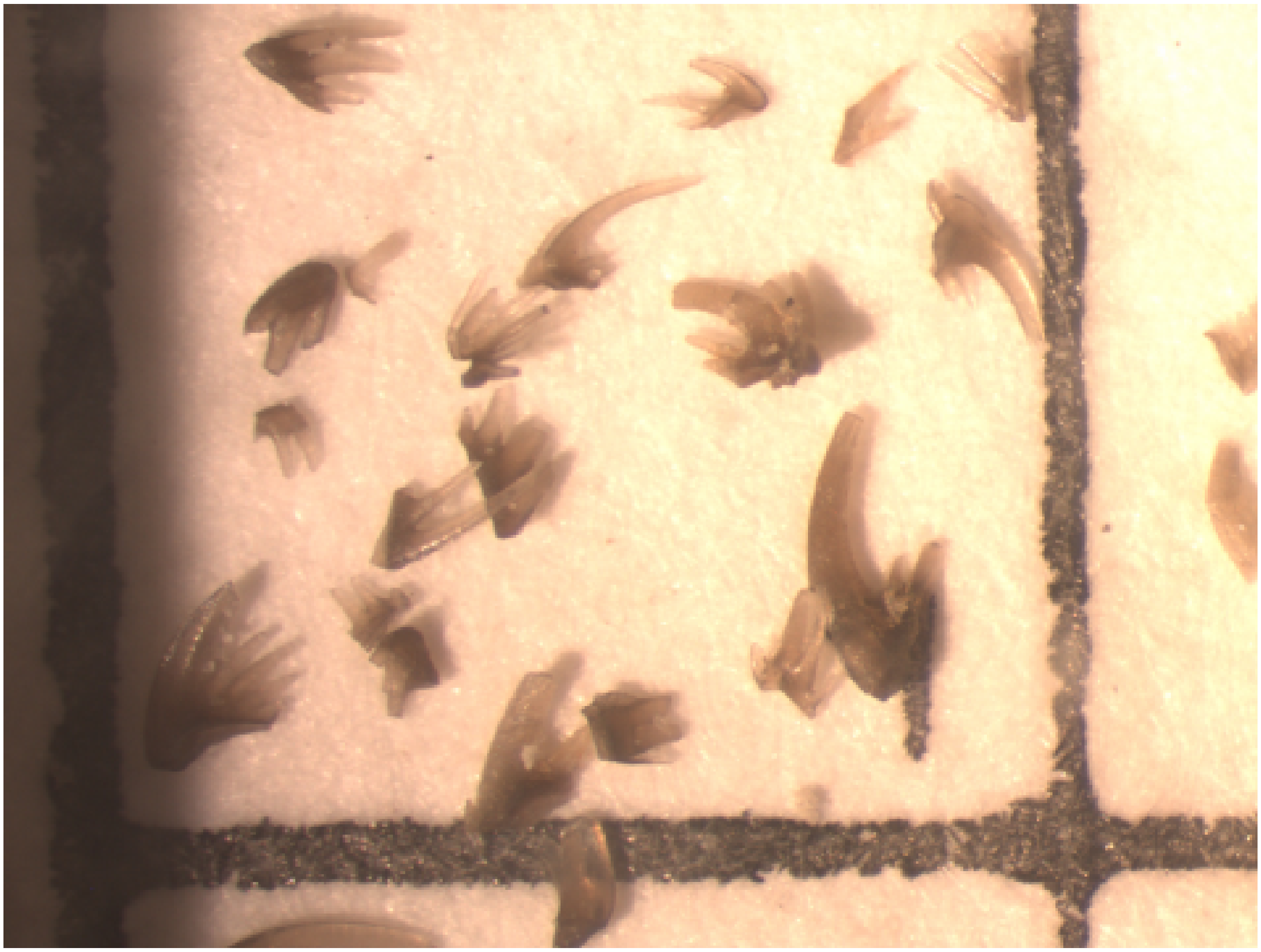

Fig. S2.c Antelope Range sample 5-25-82R
Saltzman et al

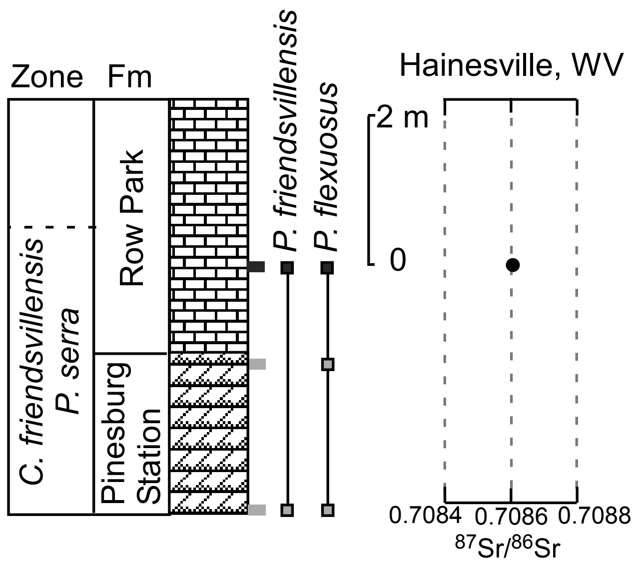

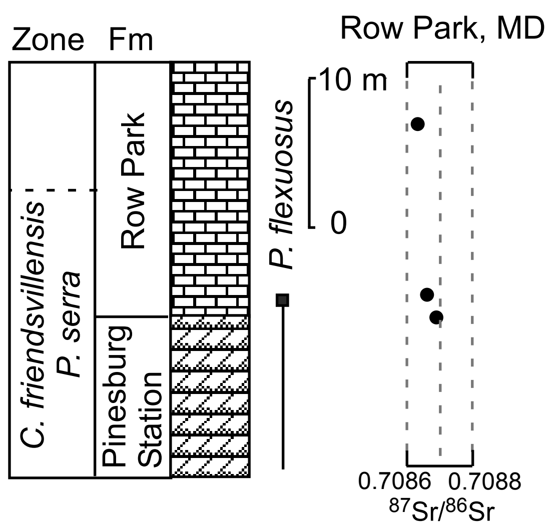

Fig. S3, Saltzman et al

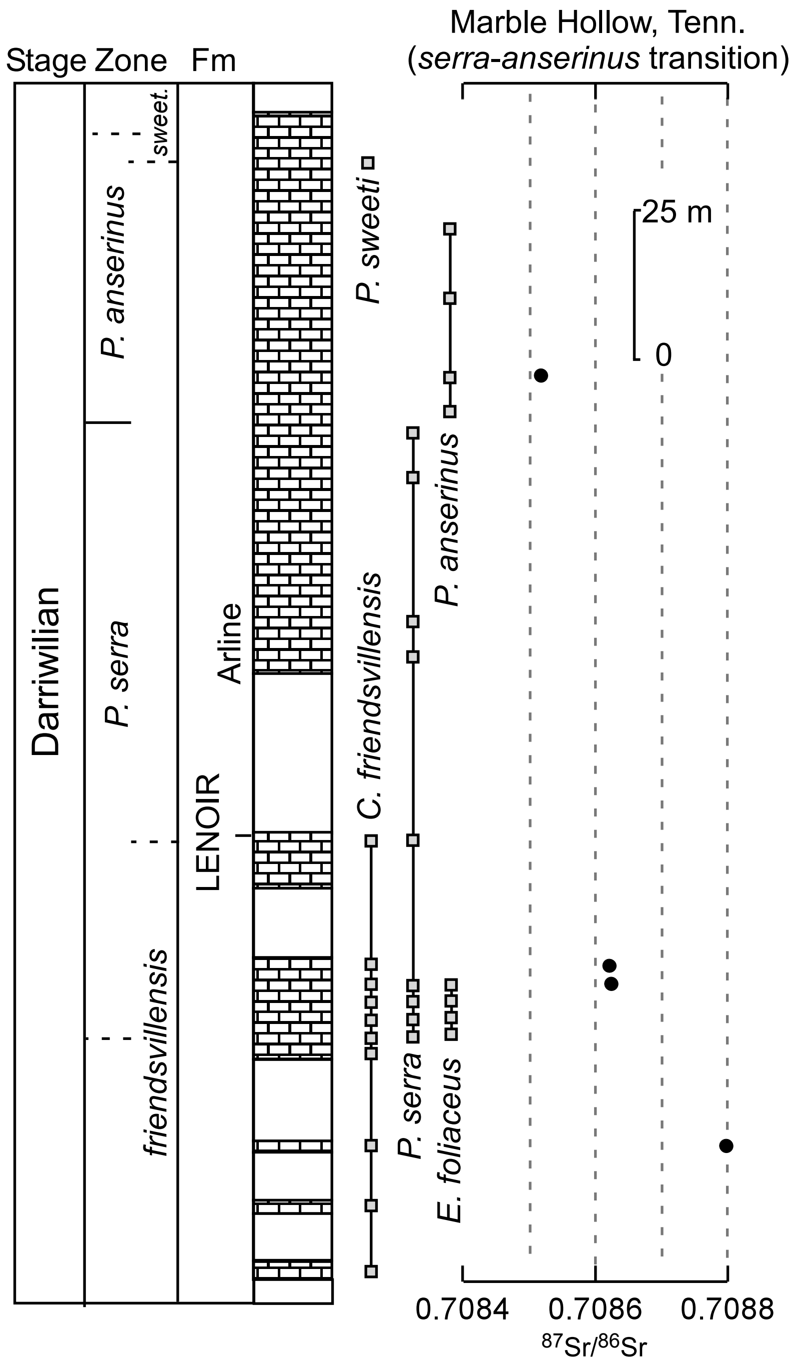

Fig. S4, Saltzman et al

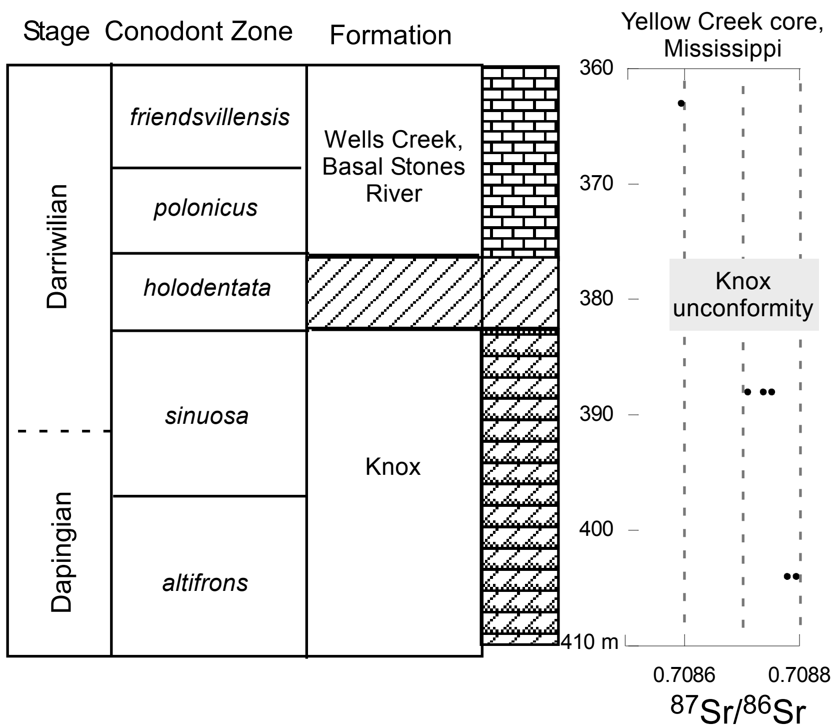

Fig. S5, Saltzman et al

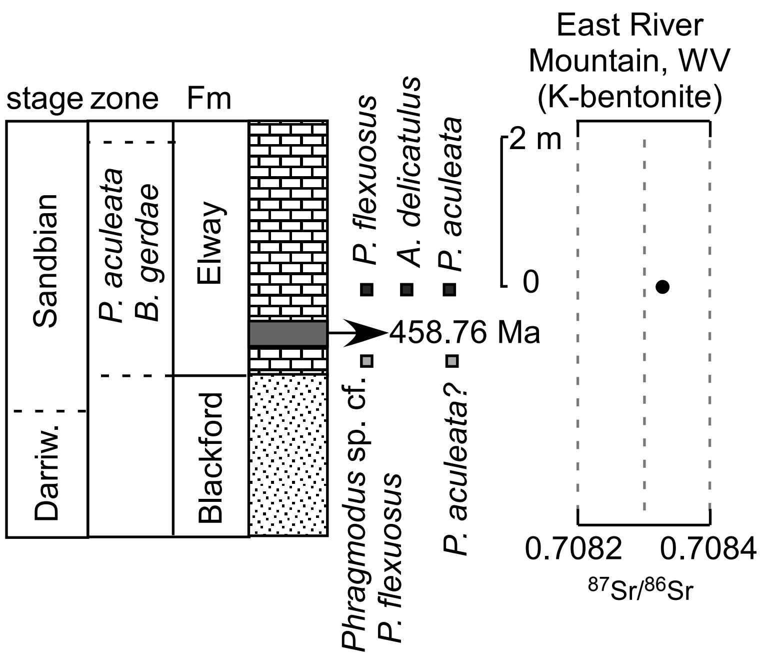

Fig. S6, Saltzman et al

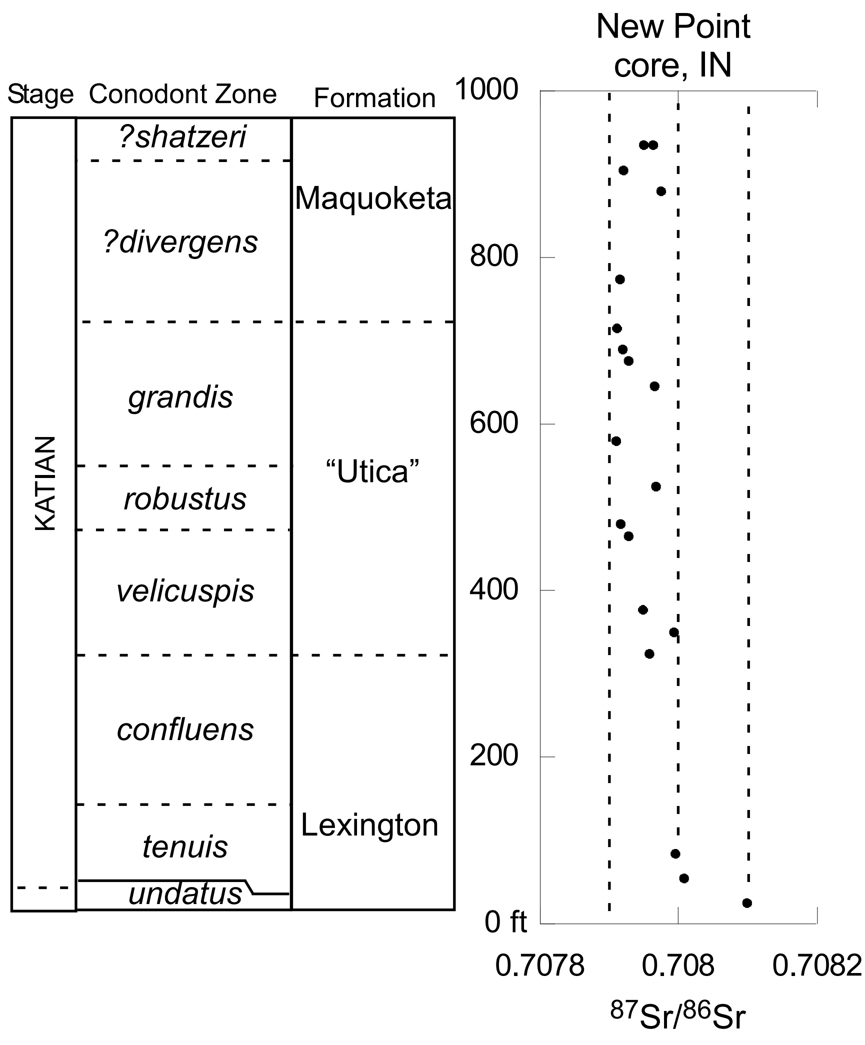

Fig. S7, Saltzman et al

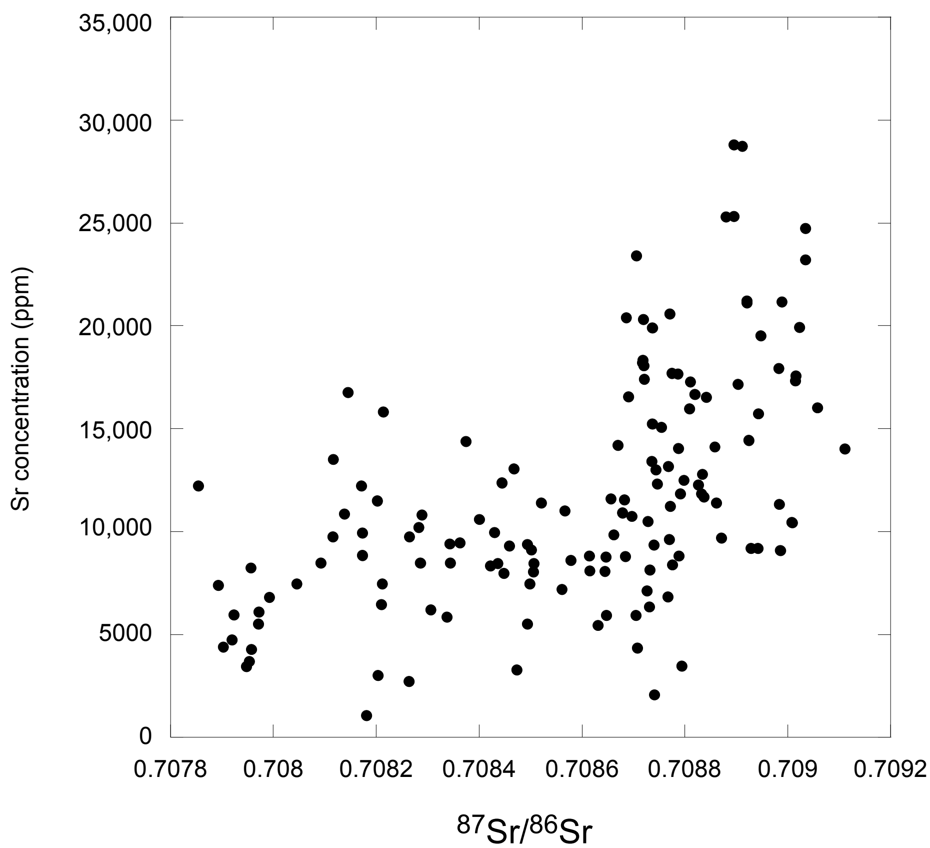

Fig. S8, Saltzman et al

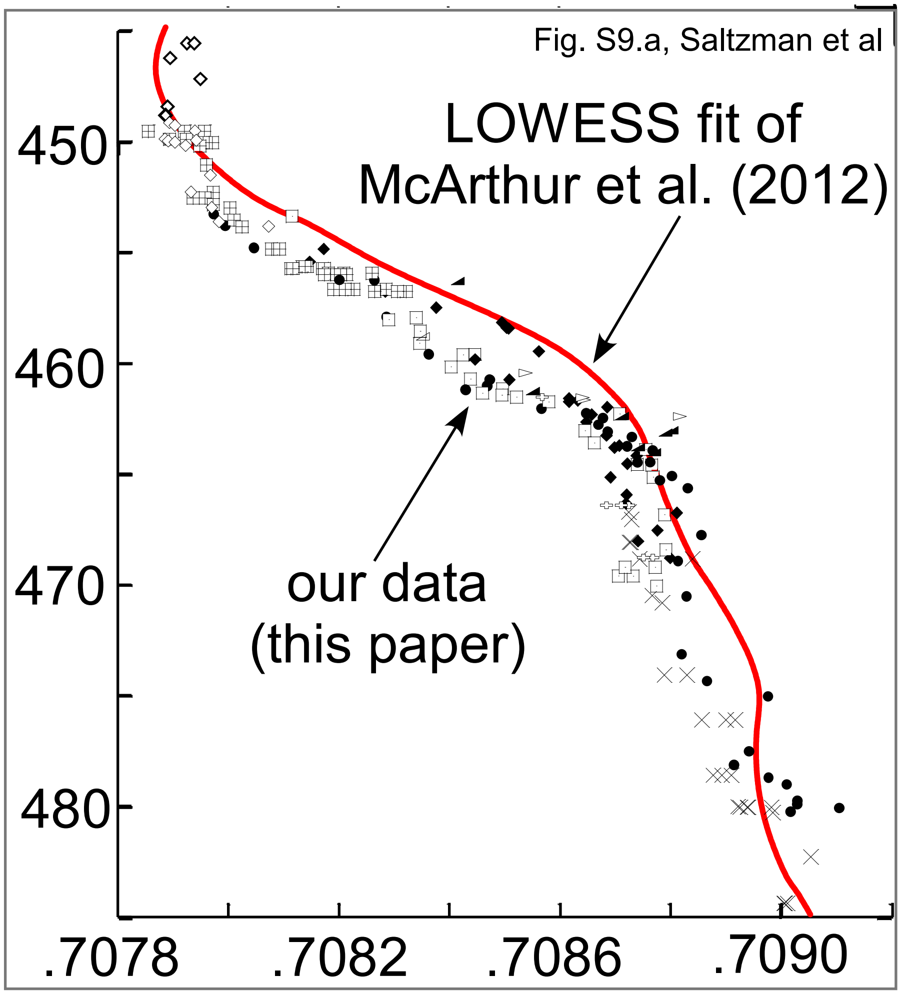
Fig. S9.a, Saltzman et al
LOWESS fit of
McArthur et al. (2012)
our data
(this paper)
450
460
470
480
.7078
.7082
.7086
.7090

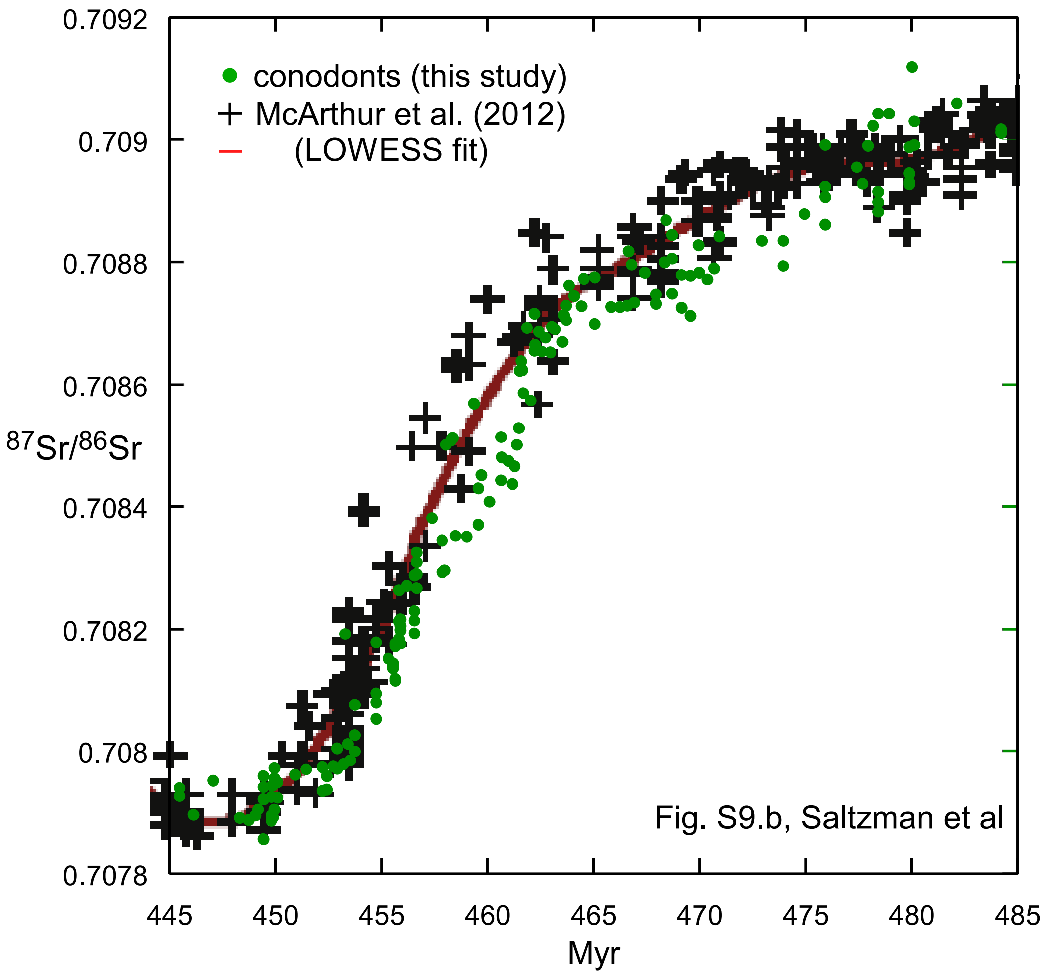
conodonts (this study)
McArthur et al. (2012)
(LOWESS fit)
Fig. S9.b, Saltzman et al
0.7092
0.709
0.7088
0.7086
0.7084
0.7082
0.708
0.7078
87Sr/86Sr
445
450
455
460
465
470
475
480
485
Myr

TABLE S1 - Sr ISOTOPE DATA

Sample ID / Locality	Meters	Uncorrected $^{87}Sr/^{86}Sr$	Uncertainty ($x\ 10^{-6}$)	ppm (conc.) Sr	*Corrected $^{87}Sr/^{86}Sr$	Age (Ma)
***Corrected values** are to a preferred value for SRM 987 of 0.710245; note that these corrected values are only plotted in the compilation Figs. 11 and 12 (see text) to account for inter-laboratory bias between Ohio State (OSU) and North Carolina (UNC). The amount of the correction was to add 0.000021 to OSU data and subtract 0.000024 from UNC data, which would fall within the symbols used to plot data points in Figs. 4-10.						
I-35, Oklahoma (OSU) - CAI = 1-2						
72SB-13	0.0	0.708779	11	12441	0.708800	468.75
72SB-139	38.4	0.708720	9	9309	0.708741	468.00
72SB-239	68.9	0.708756	9	8341	0.708777	467.50
72SB-365	107.0	0.708791	13	17230	0.708812	466.73
72SC-120	143.6	0.708699	8	18287	0.708720	466.30
72SC-220	174.1	0.708700	12	20272	0.708721	465.90
72SC-390	225.9	0.708671	10	16505	0.708692	465.10
72SC-500	259.5	0.708701	12	18022	0.708722	464.51
72SC-630	299.1	0.708718	9	19870	0.708739	464.13
83JD-20	320	0.708678	10	10686	0.708699	463.77
83JD-21	321	0.708686	8	23373	0.708707	463.68
83JD-26	326	0.708663	8	11508	0.708684	463.24
83JD-33	333	0.708627	7	8722	0.708648	462.62
83JD-42	342	0.708637	7	11546	0.708658	462.30
83JD-80	380	0.708665	17	8750	0.708686	461.94
83JD-104	404	0.708596	8	8041	0.708617	461.72
83JD-110	410	0.708611	12	5392	0.708632	461.66
83JD-120	420	0.708595	9	8782	0.708616	461.57
83JD-166	466	0.708487	13	8411	0.708508	460.72
83JD-184	484	0.708425	6	12323	0.708446	459.80
83JD-191	491	0.708541	7	7159	0.708562	459.44
83JD-211	511	0.708486	7	7997	0.708507	458.41
83JE-0.8	511.8	0.708482	10	9072	0.708503	458.37
83JE-5.6	516.6	0.708474	11	9337	0.708495	458.12
83JE-18.5	529.5	0.708355	9	14348	0.708376	457.46
83JE-33	544	0.708263	8	10159	0.708284	456.72
83JE-66	577	0.708125	9	16737	0.708146	455.40
83JE-81	592	0.708151	8	12172	0.708172	454.80
Shingle Pass, NV (OSU) - CAI = 3.5-5						
SP300	91.46	0.709003	12	19891	0.709024	480.22
SP573	174.70	0.709092	9	13967	0.709113	480.11
SP991	302.13	0.709015	9	24696	0.709036	479.94
SP1042	317.68	0.709015	10	23173	0.709036	479.72
SP1200	365.85	0.708996	11	17531	0.709017	479.02
SP1277	389.33	0.708963	11	17889	0.708984	478.68
SP1402	427.44	0.708901	9	21173	0.708922	478.13
SP1540	469.51	0.708928	9	19473	0.708949	477.52
SP1760	536.59	0.708964	29	11276	0.708985	475.01
SP1820	554.88	0.708851	13	9647	0.708872	474.33

SP1980	603.66	0.708807	11	12222	0.708828	473.12
SP2404	732.93	0.708815	7	12738	0.708836	470.52
SP2653	808.84	0.708800	10	16621	0.708821	468.90
SP2848	868.29	0.708842	12	11355	0.708863	467.73
SP-212	1084	0.708817	12	11635	0.708838	465.63
SP-237	1109	0.708767	12	17635	0.708788	465.25
SP-248.5	1120.5	0.708789	21	15918	0.708810	465.08
SP-290	1162	0.708749	13	13119	0.708770	464.46
SP-366	1238	0.708716	8	13365	0.708737	463.32
Antelope Range, NV (OSU) - CAI = 1-2; see Fig. S2 photos						
5-15-78Q	297.62	0.708724	10	12968	0.708745	464.5
5-15-78P	304.94	0.708751	19	20532	0.708772	464
5-25-82A	313.78	0.708702	11	17350	0.708723	463.77
5-25-82J	320.18	0.708667	6	20350	0.708688	463.10
5-25-82N	322.93	0.708650	11	14144	0.708671	462.81
5-25-82R	325.98	0.708659	8	10875	0.708680	462.50
5-25-82U	329.94	0.708628	12	5879	0.708649	462.29
5-25-82AB	333.90	0.708547	6	10961	0.708568	462.08
8-8-75B	350.37	0.708410	13	9923	0.708431	461.23
5-25-82AI	352.50	0.708448	9	13005	0.708469	461.05
5-25-82AK	355.85	0.708454	17	3233	0.708475	460.76
5-26-82A	368.96	0.708343	10	9418	0.708364	459.63
5-26-82M	388.78	0.708266	7	8432	0.708287	457.93
8-8-75F	414.39	0.708244	14	2676	0.708265	456.26
8-8-75Fb	414.39	0.708184	21	2973	0.708205	456.26
5-26-82AS	425.98	0.708026	13	7425	0.708047	454.80
8-8-75I	472.93	0.707973	10	6765	0.707994	453.81
5-15-78J	482.07	0.707952	19	6069	0.707973	453.29
Clear Spring, MD (OSU) - CAI = 4-5			0			
I70-9	9	0.708755	12	17649	0.708776	470.06
I70-20	20	0.708685	10	5891	0.708706	469.62
I70-20b	20	0.708718	6	15209	0.708739	469.62
I70-30.2	30.2	0.708752	12	11193	0.708773	469.22
I70-30.2b	30.2	0.708698	8	18171	0.708719	469.22
CS-50	50	0.708775	19	3424	0.708796	468.43
CS-90	90	0.708769	20	8779	0.708790	466.85
CS-122	122	0.708748	24	6771	0.708769	465.14
CS-130	130	0.708721	21	2012	0.708742	464.59
I70-140	140	0.708735	14	15030	0.708756	463.91
I70-146	146	0.708642	14	9790	0.708663	463.59
I70-152	152	0.708625	44	8020	0.708646	463.06
I70-166	166	0.708688	13	4317	0.708709	462.29
I70-220	220	0.708559	18	8569	0.708580	461.74
I70-240	240	0.708501	11	11346	0.708522	461.54
I70-250	250	0.708474	10	5482	0.708495	461.44
I70-260	260	0.708439	9	9270	0.708460	461.33
I70-270	270	0.708479	13	7418	0.708500	461.23
I70-280	280	0.708417	35	8409	0.708438	460.70
I70-290	290	0.708381	8	10549	0.708402	460.17

I70-300	300	0.708403	7	8288	0.708424	459.63
I70-300b	300	0.708429	19	7927	0.708450	459.63
I70-310	310	0.708324	9	9364	0.708345	459.10
I70-320	320	0.708325	11	8429	0.708346	458.57
I70-330	330	0.708269	11	10771	0.708290	458.03
I70-332	332	0.708318	8	5818	0.708339	457.93
I70-435.4	435.4	0.708096	22	9691	0.708117	453.35
Meiklejohn Peak, NV (OSU) - CAI = 4			0			
MP-18	322	0.708757	19	8542	0.708778	464.00
5-8-78-O	398.4	0.708727	12	6370	0.708748	463.77
5-8-78-I	449.9	0.708778	9	4476	0.708799	463.10
5-8-78-H	456	0.708788	12	5895	0.708809	463.00
5-7-78Q	538.9	0.708698	18	10033	0.708719	462.35
5-7-78-M	560.28	0.708537	10	10186	0.708558	461.23
5-7-78-L	568.5	0.708401	10	6882	0.708422	456.26
Marble Hollow, TN (OSU); only plotted in Fig. 11; see Fig. S4						
MH64B7-6	22.5	0.708799	11	4237	0.708820	462.35
68B5-5	49.5	0.708626	9	4754	0.708647	461.6
MH70B29-2	52.5	0.708623	21	3930	0.708644	461.5
69B2-5	163.5	0.708520	16	31325	0.708541	460.4
East River Mountain (OSU); only plotted in Fig. 11; see Fig. S6						
ERMBent	0	0.708341	8	9639	0.708362	458.76
Cominco core, KY (UNC) - CAI = 1-2						
	363	0.707880		12190	0.707856	449.50
	363	0.707945		4700	0.707921	449.50
	363	0.707982		8210	0.707958	449.50
	335	0.707919		7342	0.707895	449.86
	335	0.707949		5902	0.707925	449.86
	319	0.707996		5483	0.707972	450.00
	319	0.707979		3652	0.707955	450.00
	284	0.707973		3398	0.707949	450.15
	266	0.707985			0.707961	451.00
	232	0.707997			0.707973	452.27
	214	0.707961			0.707937	452.50
	214	0.707983		4225	0.707959	452.50
	198	0.707998			0.707974	452.80
	186	0.708028			0.708004	452.97
	173	0.708035			0.708011	453.50
	167	0.708050			0.708026	453.81
	150	0.708103			0.708079	454.80
	150	0.708118		8444	0.708094	454.80
	91	0.708159			0.708135	455.60
	91	0.708167			0.708143	455.60
	91	0.708164		10813	0.708140	455.60
	82	0.708138			0.708114	455.70
	82	0.708142		13463	0.708118	455.70
	73	0.708195			0.708171	455.70
	73	0.708199		9894	0.708175	455.70
	66	0.708286			0.708262	455.90

	66	0.708235	6413	0.708211	455.90
	66	0.708206	1027	0.708182	455.90
	54	0.708221		0.708197	455.95
	54	0.708239	15785	0.708215	455.95
	54	0.708199	8800	0.708175	455.95
	54	0.708228	11454	0.708204	455.95
	30	0.708253		0.708229	456.62
	30	0.708311		0.708287	456.62
	30	0.708216		0.708192	456.62
	30	0.708237	7425	0.708213	456.62
	25	0.708348		0.708324	456.72
	25	0.708290	9702	0.708266	456.72
	25	0.708332	6143	0.708308	456.72
New Point core, IN (UNC) - CAI = 1-2; only plotted in Fig. 11; see Fig. S7					
	285	0.707950		0.707926	445.53
	285	0.707963		0.707939	445.53
	276	0.707920		0.707896	446.20
	268	0.707975		0.707951	447.14
	236	0.707915		0.707891	448.40
	218	0.707911		0.707887	448.80
	210	0.707919		0.707895	449.12
	206	0.707928	4348	0.707904	449.25
	197	0.707965		0.707941	449.50
	177	0.707910		0.707886	449.86
	160	0.707967		0.707943	449.92
	146	0.707916		0.707892	449.95
	142	0.707928		0.707904	450.00
	115	0.707948		0.707924	450.15
	107	0.707993		0.707969	451.50
	99	0.707958		0.707934	452.27
	26	0.707995		0.707971	452.97
	16	0.708008		0.707984	453.60
	8	0.708099		0.708075	453.81
	8	0.708099		0.708075	453.81
Yellow Creek, MS (UNC); only plotted in Fig. 11; see Fig. S5					
	363	0.708594	4582	0.708570	461.5
	388	0.708710	3947	0.708686	466.38
	388	0.708751	3814	0.708727	466.38
	388	0.708737	5786	0.708713	466.38
	404	0.708794	9835	0.708770	468.75
	404	0.708778	5952	0.708754	468.75
Oklahoma (UNC) - CAI = 1-2					
Chapman Ranch	1584	0.708867	16486	0.708843	468.75
Chapman Ranch	1584	0.708772	12274	0.708748	468.75
Chapman Ranch	1430	0.708813	14016	0.708789	470.75
Chapman Ranch	1250	0.708929	17123	0.708905	476.00
Chapman Ranch	1250	0.708946	21087	0.708922	476.00
Chapman Ranch	1250	0.708884	14083	0.708860	476.00
Chapman Ranch	1016	0.708938	28690	0.708914	478.50

Chapman Ranch	1016	0.708921	28745	0.708897	478.50
Chapman Ranch	1016	0.708921	25279	0.708897	478.50
Chapman Ranch	1016	0.708905	25268	0.708881	478.50
Chapman Ranch	773	0.708950	14396	0.708926	479.94
Chapman Ranch	616	0.708954	9136	0.708930	479.96
Chapman Ranch	616	0.708969	15694	0.708945	479.96
Chapman Ranch	616	0.709011	9056	0.708987	479.96
Chapman Ranch	616	0.708967	9145	0.708943	479.96
I-35	255	0.709014	21131	0.708990	480.20
I-35	206	0.709083	15970	0.709059	482.20
I-35	53	0.709040	17277	0.709016	484.28
I-35	53	0.709035	10388	0.709011	484.28
I-35	53	0.709034	10394	0.709010	484.28
Hwy-77	140	0.708752	7080	0.708728	466.65
Hwy-77	115	0.708757	8110	0.708733	467.00
Hwy-77	34	0.708756	6300	0.708732	468.00
Sycamore Creek	117	0.708754	10458	0.708730	468.00
Sycamore Creek	87	0.708795	9577	0.708771	470.42
Sycamore Creek	42	0.708817	11792	0.708793	474.00
Sycamore Creek	42	0.708858	11787	0.708834	474.00

TABLE S2 - SUPPLEMENTAL DATA (see Fig. S3)

Sample ID / Locality	**Meters**	**Uncorrected $^{87}Sr/^{86}Sr$**	**Uncertainty ($\times 10^{-6}$)**	**ppm Sr**
Row Park, MD (OSU)				
74JB1-16	-0.30	0.708693	11	5352
74JB1-9	0.30	0.708644	13	5233
74JB1-11	9.15	0.708621	12	6569
Hainesville, WV (OSU)				
74JB5-4	1	0.708604	13	10215

TABLE S3 - INTERLABORATORY COMPARISON

Sample ID	*Duke University	Ohio State University	Difference (Duke-OSU)
83JD-42	0.708661	0.708637	0.000024
SP-300r	0.709068	0.709038	0.000030
SP-300c	0.709043	0.709003	0.000040
5-25-82AI	0.708467	0.708448	0.000019
74JB1-9	0.708622	0.708644	-0.000022
Standard	**Long term average**		
NIST SRM 987	0.710269	0.710224	0.000045

*Note that Duke University is the current home of G. Dwyer (samples for Dwyer's 1996 PhD thesis were run at Univ of North Carolina)

TABLE S4 - DUPLICATE SAMPLE ANALYSES

Sample ID	**$^{87}Sr/^{86}Sr$**	**Difference (x 10^{-6})**
8-8-75Fa	0.708244	60
8-8-75Fb	0.708184	
I70-20a	0.708685	33
I70-20b	0.708718	
I70-30.2a	0.708752	54
I70-30.2b	0.708698	
I70-300a	0.708403	26
I70-300b	0.708429	
CC-363a	0.707880	
CC-363b	0.707945	102
CC-363c	0.707982	
CC-335a	0.707919	30
CC-335b	0.707949	
CC-319a	0.707996	17
CC-319b	0.707979	
CC-214a	0.707961	22
CC-214b	0.707983	
CC-150a	0.708103	15
CC-150b	0.708118	
CC-91a	0.708159	
CC-91b	0.708167	8
CC-91c	0.708164	
CC-82a	0.708138	4
CC-82b	0.708142	
CC-73a	0.708195	4
CC-73b	0.708199	

Sample ID	**$^{87}Sr/^{86}Sr$**	**Difference (x 10^{-6})**
CC-66a	0.708286	
CC-66b	0.708235	80
CC-66c	0.708206	
CC-54a	0.708221	
CC-54b	0.708239	40
CC-54c	0.708199	
CC-54d	0.708228	
CC-30a	0.708253	
CC-30b	0.708311	95
CC-30c	0.708216	
CC-30d	0.708237	
CC-25a	0.708348	
CC-25b	0.708290	58
CC-25c	0.708332	
NP-285a	0.707950	13
NP-285b	0.707963	
NP-8a	0.708099	0
NP-8b	0.708099	
CR-1584a	0.708867	95
CR-1584b	0.708772	
CR-1250a	0.708929	
CR-1250b	0.708946	62
CR-1250c	0.708884	
CR-1016a	0.708938	
CR-1016b	0.708921	33
CR-1016c	0.708921	
CR-1016d	0.708905	
CR-616a	0.708954	
CR-616b	0.708969	57
CR-616c	0.709011	
CR-616d	0.708967	
I35-53a	0.709040	
I35-53b	0.709035	6
I35-53c	0.709034	
SC-42a	0.708817	41
SC-42b	0.708858	

Total:	24
Minimum(x 10^{-6}):	0
Maximum(x 10^{-6}):	102
Average(x 10^{-6}):	40
Std. Dev.(x 10^{-6}):	31

Calibration of a conodont apatite-based Ordovician $^{87}Sr/^{86}Sr$ curve to biostratigraphy and geochronology: Implications for stratigraphic resolution

The following represents a more complete version of what appears in the Discussion section of the paper under the same subheading:

Ordovician Sr isotope stratigraphy and stratigraphic resolution

For parts of the Ordovician when rates of change in $^{87}Sr/^{86}Sr$ are relatively high (~ 5.0 to 10.0 x 10^{-5} per myr), Sr isotope stratigraphy (SIS) is likely to be useful as a high resolution tool for correlation that is on par with, or potentially better than, conodont biostratigraphy. This is especially true for rocks that only preserve long-ranging conodonts or conodont species that have poorly constrained age rages, such as those at the Clear Spring section where there are low yields of shallow-water Midcontinent Realm conodonts in dominantly tidal to shallow subtidal facies. Maximum stratigraphic resolution using $^{87}Sr/^{86}Sr$ is limited by sample reproducibility of Ordovician conodonts. Our study indicates that samples run in duplicate are on average different by 4.0 x 10^{-5} with a 2σ standard deviation of 6.2 x 10^{-5} (Table S4). Thus, if duplicate or stratigraphically adjacent samples are analyzed, it may be possible in the best case scenario to subdivide parts of the Ordovician into Sr isotope ‘slices’ of approximately 0.5 to 1.0 myr resolution (i.e., during a 1 myr time period in which $^{87}Sr/^{86}Sr$ changed by 8.0 x 10^{-5}, it may be possible to resolve two distinct 0.5 myr intervals – see Table 1 and Fig. 12). Table 1 compares resolution possible with Sr isotope stratigraphy and conodont zones, and in Fig. 12 we show an example of how SIS can be used in the Ordovician. Fig. 12 utilizes Oklahoma $^{87}Sr/^{86}Sr$ data only in an effort to eliminate scatter in the curve from uncertainty in relative positioning of samples from different regions within individual conodont zones (which is a significant source of uncertainty in the North American compilation in Fig. 11). In Fig. 12, the potential resolution in different parts of the Ordovician curve at high versus low rates of $^{87}Sr/^{86}Sr$ change is depicted, as are the best and worst case scenarios (i.e., depending on whether a duplicate analysis is run, and whether the assumed $^{87}Sr/^{86}Sr$ precision is based on the average difference or 2σ standard deviation).

The Ordovician absolute time scale (Cooper and Sadler, 2012) and placement of an individual sample accurately within a conodont zone (Table 1) are also sources of error in calculating rates of change in $^{87}Sr/^{86}Sr$, which in turn affect estimates of potential stratigraphic resolution (Fig. 12). In the discussion that follows we use the durations of Ordovician stages and conodont zones from Cooper and Sadler (2012) to estimate potential stratigraphic resolution.

The resolution of SIS in Lower Ordovician stages (Tremadocian-Floian) is relatively low compared to more rapidly changing parts of the Middle and Upper Ordovician $^{87}Sr/^{86}Sr$ curve (Table 1; Figs. 11, 12). The $^{87}Sr/^{86}Sr$ value for the base of the Lower Ordovician is ~ 0.70905 and the base of the Middle Ordovician is 0.70880 in Nevada (Shingle Pass) and Oklahoma. The calculated Lower Ordovician $^{87}Sr/^{86}Sr$ rate of fall ~ 1.6×10^{-5} per myr (note that some potential structure on this overall fall may be substantiated with future work) is similar to other slowly changing time periods in the Phanerozoic such as the early Cenozoic (McArthur et al., 2012). Using our best estimate of ~ 4.0×10^{-5} for sample precision (see Table S3, S4), it is possible to subdivide the Lower Ordovician into about 6 resolvable Sr isotope 'slices' of about 2-3 myr each. This resolution is somewhat less than that provided by the roughly 9 conodont zones (Cooper and Sadler, 2012) that average 1.7 myr in duration (Table 1; Fig. 12).

For the Middle Ordovician, $^{87}Sr/^{86}Sr$ falls from 0.70880 to 0.70875 within the Dapingian Stage (Figs. 11, 12), which represents 2.7 myr (Cooper and Sadler, 2012). The calculated

Dapingian rate of change is 1.9 x 10^{-5} per myr and thus similar to the Lower Ordovician (Table 1). Even if we place the top of the Dapingian at 0.70870 which is possible resulting from uncertainty in biostratigraphy, the rate of change goes up to ~ 3.7 x 10^{-5} per myr but the resolving power using SIS is still not much different than conodont zones (3 conodont zones are included in the Dapingian, with an average resolution of 0.9 myr). The possibility of an older age for the base of the Dapingian at 473 myr (Thompson and Kah, 2012; Thompson et al., 2012) would result in a longer duration for the Dapingian and shorter Lower Ordovician, making rates of change in $^{87}Sr/^{86}Sr$ similarly slow for both intervals.

The Middle Ordovician Darriwilian Stage represents a critical time period in which the rate of fall in $^{87}Sr/^{86}Sr$ steepens significantly. If the base of the Darriwilian is taken from near the Joins-Oil Creek formation transition in Oklahoma at 0.70875 and the top from the upper part of the *C. sweeti* zone at 0.70835 (Figs. 11, 12), then this $^{87}Sr/^{86}Sr$ change over the 8.9 myr duration of the Darriwilian (Cooper and Sadler, 2012) results in a drop of 4.5 x 10^{-5} per myr (a similar rate of fall is observed in parts of the late Cenozoic; McArthur et al., 2012). The dates of Thompson et al. (2012) raise the possibility that the base of the Darriwilian could be as old as 469 myr and would lower the $^{87}Sr/^{86}Sr$ rate of change to 3.5 x 10^{-5} per myr (ages for the middle and top of the Darriwilian seem unlikely to move by more than 1-2 myr based on the dates in Sell et al., 2011). Assuming a rate of change of ~ 4.5 x 10^{-5} per myr over about 8.9 myr for the Darriwilian, it may be possible to discern about 10 Sr isotope 'slices' with an average resolution of 0.9 myr compared to 5 conodont zones with an average resolution of 1.8 myr (Table 1).

The Sandbian $^{87}Sr/^{86}Sr$ change is from 0.70835 to 0.70800 in 5.4 myr and the calculated rate of change at 6.5 x 10^{-5} per myr is higher than the Darriwilian. There are about 9 possible Sr isotope 'slices' in the Sandbian with 0.6 myr resolution compared to about 5 conodont zones with an average resolution of 1.1 myr (Table 1). Rates of change in $^{87}Sr/^{86}Sr$ slow dramatically in the Katian Stage until the curve reverses course and begins to rise somewhere in the upper part of the Katian through the terminal Ordovician Hirnantian Stage. Use for SIS is thus more limited in the 7.8 myr long Katian (average resolution of a Sr isotope 'slice' is 3.1 myr compared to 7 conodont zones with average resolution of 1.1 myr), although it may be possible to recognize the turnaround from falling to rising $^{87}Sr/^{86}Sr$ as a marker horizon in long continuous stratigraphic sections.

Calibration of $^{87}Sr/^{86}Sr$ to mid Darriwilian to mid Sandbian conodont zones

$^{87}Sr/^{86}Sr$ stratigraphy has great potential to improve global correlations in parts of the Darriwilian and Sandbian with average rates of change between ~ 4.5 to 6.5 x 10^{-5} per myr (Table 1; Figs. 11, 12). Here we focus in greater detail on $^{87}Sr/^{86}Sr$ rates of change as calculated for individual conodont zones in this time interval that in some cases greatly exceed these averages and are on par with some of the highest rates in the Phanerozoic such as the Late Cenozoic, Middle Jurassic or Early Triassic (Fig. 1; McArthur et al., 2012). The time resolution possible using $^{87}Sr/^{86}Sr$ varies not only with the rate of change but also with how well calibrated the curve is to biostratigraphy and geochronology, and in the sections below we use the well-studied sections in Oklahoma as the primary reference standard in calibration of the $^{87}Sr/^{86}Sr$ curve to conodont zones unless otherwise noted.

The *E. variabilis* and *H. holodentata* conodont zones of the middle Darriwilian are 2.61 myr (Cooper and Sadler, 2012) and $^{87}Sr/^{86}Sr$ changes from less than ~ 0.70880 to 0.70875 for a maximum rate of change of 1.9 x 10^{-5} per myr (Table 1). This rate of change is similar to the average rate for the preceding Lower and Middle Ordovician time interval, and thus represents a baseline $^{87}Sr/^{86}Sr$ rate of change for comparison with subsequent zones. The next younger conodont zone is the North Atlantic *E. suecicus* Zone of the middle Darriwilian (within stage slice Dw2 of Bergström et al., 2009). The *E. suecicus* zone is 1.27 myr (Cooper and Sadler, 2012) and $^{87}Sr/^{86}Sr$ changes from 0.70875 to 0.70865 for a significant increase in the rate of change to 7.9 x 10^{-5} per myr. The partly time equivalent North American Midcontinent *P. polonicus* Zone is slightly longer at 1.42 myr and may reach 0.70860 at the top yielding a rate of change of 10.5 x 10^{-5} per myr that is among the highest in the Phanerozoic. However, despite the potential to subdivide the *E. suecicus* and *P. polonicus* zones into between 2 and 4 Sr isotope 'slices' of 0.4 to 0.5 myr resolution (Table 1), the number of $^{87}Sr/^{86}Sr$ data points used to calibrate these zones is relatively limited (based on a single data point at Meiklejohn Peak and two data points in a thin interval near the base of the McLish Formation in Oklahoma for the *P. polonicus* zone, and three data points at Meiklejohn Peak in Nevada for the *E. suecicus* zone; Figs. 5, 8).

The *P. serra* Zone (marking the base of Dw3 of Bergström et al., 2009) is 1.99 myr (Cooper and Sadler, 2012) and the $^{87}Sr/^{86}Sr$ change from 0.70865 to 0.70852 is well defined by two data points at Marble Hollow in Tennessee (Figs. 11, S4) that capture the transition to the overlying *P. anserinus* Zone, as well as three data points in the Antelope Range of Nevada and two in Oklahoma (from *E. foliaceus* Subzone). The *P. serra* Zone rate of change of 6.5 x 10^{-5} per myr and the average resolution possible with SIS is comparable to underlying zones (Table 1). The *Cahabagnathus friendsvillensis* Zone is shorter than the partly time equivalent *P. serra* Zone at 1.12 myr and falls near 0.70860 at the bottom and 0.70850 at the top yielding a rate of change of 8.9 x 10^{-5} per myr and potential 0.4 myr resolution. $^{87}Sr/^{86}Sr$ data directly from the *C. friendsvillensis* Zone includes seven horizons in the McLish and Tulip Creek formations of

Oklahoma (including the ranges of *C.* n. sp. and *C. directus*), one data point each in the St. Paul Group of Maryland and the top Antelope Valley Limestone in Nevada, and two in the section at Marble Hollow.

The *P. anserinus* Zone, which includes the base of the Sandbian (Sa1 Stage Slice) within it, is 2.58 myr (Cooper and Sadler, 2012) and $^{87}Sr/^{86}Sr$ changes from 0.70852 to 0.70832 yielding a rate of change of 7.8×10^{-5} per myr and 0.5 myr resolution possible with SIS (Table 1). $^{87}Sr/^{86}Sr$ directly from stratigraphic horizons yielding conodonts of the *P. anserinus* zone include one data point in the section at Marble Hollow (Figs. 11, S4) which closely approximates the base of the zone, as well as one data point in Nevada (possibly more depending on discrepancy of first occurrence of *P. anserinus* in Harris et al., 1979 versus Sweet et al., 2005). The *C. sweeti* Zone is longer than the partly time equivalent *P. anserinus* Zone at 4.51 myr and falls near 0.70850 at the bottom and 0.70830 at the top yielding a rate of change of 4.4×10^{-5} per myr and 0.9 myr resolution with SIS. Data directly from stratigraphic horizons yielding conodonts of the *C. sweeti* Zone include three data points in the Tulip Creek and Bromide formations of Oklahoma, and four data points in the Copenhagen Formation in Nevada. However, considerable uncertainty exists in placement of the top of the *C. sweeti* Zone. The Cominco core in the type Cincinnati region contains the overlying *Plectodina aculeata* Zone with a value of ~ 0.70830, consistent with where the top of the *C. sweeti* Zone should fall in the Copenhagen Formation in Nevada and the Bromide Formation in Oklahoma.

The *B. variabilis* Zone is 1.67 myr and $^{87}Sr/^{86}Sr$ changes from 0.70832 to ~ 0.70822 at the base of *B. gerdae* Zone yielding a rate of change of 6.0×10^{-5} per myr and the potential for 0.7 myr resolution with SIS (Table 1). $^{87}Sr/^{86}Sr$ data directly from stratigraphic horizons yielding conodonts of the *B. variabilis* Zone are absent, but if we use *E. elongatus* as a proxy for this zone, then there are two points from the Bromide Formation in Oklahoma and one data point in the Antelope Range in Nevada. The $^{87}Sr/^{86}Sr$ value at the base of the *B. gerdae* Zone (close to the base of Stage Slice Sa2; Bergström et al., 2009) is problematic because calibration is based on single data points in the Antelope Range and Meiklejohn Peak sections that show significant disagreement (the more radiogenic value of about 0.70840 at Meiklejohn Peak could reflect uncertainty in conodont identifications; Harris et al., 1979). The partly equivalent *P. aculeata* zone is 0.82 myr (Cooper and Sadler, 2012) and falls near 0.70830 at the bottom and 0.70815 at the top yielding an anomalously high rate of change of 18.3 x 10^{-5} per myr (Table 1). This high rate of change is likely an artifact because it is problematic to calibrate $^{87}Sr/^{86}Sr$ to conodonts of the *P. aculeata* Zone due in part to uncertainty over taxonomy of *P. aculeata* s.s. and s.l. and limited data on where to place the top and bottom of the zone (the overlying *E. quadridactylus* Zone yields a value of about 0.70815 at the base in the Cominco core; Figs. 10, 11).